Journal of Applied Fluid Mechanics, Vol. 11, No. 3, pp. 787-799, 2018.
Available online at www.jafmonline.net, ISSN 1735-3572, EISSN 1735-3645.
DOI: 10.29252/jafm.11.03.28347

Simulating Fluid and Structure Interaction using Exponential Basis Functions

H. Pary Abarghooei† and B. Boroomand

Department of Civil Engineering, Isfahan University of Technology, Isfahan, 84156-83111, Iran

†*Corresponding Author Email: abarghooei@cv.iut.ac.ir*

(Received August 26, 2017; accepted December 30, 2017)

ABSTRACT

In this paper a meshless method using exponential basis functions is developed for fluid-structure interaction in liquid tanks undergoing non-linear sloshing. The formulation in the fluid part is based on the use of Navier-Stokes equations, presented in Lagrangian description as Laplacian of the pressure, for inviscid incompressible fluids. The use of exponential basis functions satisfying the Laplace equation leads to a strong form of volume preservation which has a direct effect on the accuracy of the pressure field. In a boundary node style, the bases are used to incrementally solve the fluid part in space and time. The elastic structure is discretized by the finite elements and analyzed by the Newmark method. The direct use of the pressure, as the exponential of the acceleration, helps to find the loads acting on the structure in a straight-forward manner. The interaction equations are derived and used in the analysis of a tank with elastic walls. The overall formulation may be implemented simply. To demonstrate the efficiency of the solution, the obtained results are compared with those obtained from a finite elements solution using Lagrangian description. The results show that while the wave height and the oscillations of elastic walls of the two analyses are in good agreement with each other; the use of the proposed meshless analysis not only leads to accurate hydrodynamic pressure but also reduces the computational time to one-eighth of the time needed for the finite element analysis.

Keywords: Fluid-structure interaction; Meshless method; Exponential basis functions; Lagrangian description for fluids; Nonlinear sloshing.

NOMENCLATURE

A_f	amplitude of oscillation
c	constant factors
C	damping matrix
g	gravity acceleration
K	stiffness matrix
M	mass matrix
n	unit normal vector
N	shape functions matrix
p	fluid pressure
p_H	homogeneous part of pressure
P	pressure vector
U	displacement vector
$\dot{\mathbf{U}}$	velocity vector
$\ddot{\mathbf{U}}$	acceleration vector
x, y	cartesian coordinates
α_c , β_c	damping coefficients
β_N , γ_N	Newmark coefficients
ρ_f	fluid density

1. INTRODUCTION

Fluid-structure interaction is of particular importance in various applications in engineering mechanics and, especially, in the designing process of industrial systems. Examples of such systems are offshore structures, dams, fluid tanks, bridges, ships and spacecrafts. Predicting the hybrid fluid-structure system response is a complex process and in many practical cases finding an analytical solution is not possible. On the other hand, in this field, laboratory investigations are of limited ranges. Therefore many researchers have attempted to develop numerical methods to study the dynamic behavior and fluid-structure interaction.

The available methods to simulate the behavior of fluids and fluid-structures interaction can be categorized in; “mesh-based/element-based”

methods which use mesh for the discretization, and the so called "meshless" methods which do not require the standard mesh production. In the studies on fluid behavior, four well-known mesh-based methods can be found in the literature: finite differences method (FDM), finite volume method (FVM), finite element method (FEM) and boundary element method (BEM). The finite element method and the boundary element, and the combination of these two methods in solving problems of fluid-structures interaction have so far been attracting attention of many researchers (Firouz-Abadi *et al.* 2009; Wang and Wu 2011; Nguyen-Thoi *et al.* 2013; Kolaei *et al.* 2015).

Although the element-based methods yield useful and satisfactory results in the field of fluid-structure interaction, the success of these methods largely depends on the mesh quality and, consequently, on the time allocated for its generation process. Moreover, in the simulating waves and free surface of fluid, the possibility of confronting with highly distorted elements, and thus needing mesh regeneration, is not far from reality. Element distortion may occur at each time step, so regeneration of the mesh may include a large share of the calculation cost (Ma 2005). Therefore, the development of numerical methods that are less dependent on the mesh generation, in solving problems with the free surface of fluid with large deformation, has been highly regarded in many recent studies. Among the methods developed to simulate the behavior of fluids without needing mesh the Galerkin meshless method, diffusion element method, reproducing kernel particle method, smoothed particle hydrodynamics method (SPH), particle finite element method, moving-particle semi-implicit method (MPS), meshless local Petrov-Galerkin method (MLPG) can be noted (Lucy 1977; Monaghan 1994; Vuyst *et al.* 2005; Antoci *et al.* 2007; Mayrhofer *et al.* 2015; Oñate *et al.* 2004; Idelsohn *et al.* 2014; Sriram and Ma 2012).

The SPH method is one of the most widely used Lagrangian meshless methods in solving various engineering problems (Randles *et al.* 1996; Antoci *et al.* 2007; Zhang *et al.* 2017; Ren *et al.* 2017). This method can be classified into two categories in the field of computational fluid dynamics; i.e. the weakly compressible SPH (WCSPH) method and the incompressible SPH (ISPH) method (Liu *et al.* 2014 and 2016). ISPH method is particularly efficient in improving the pressure and the volume conservation field in comparison with WCSPH method (Lee *et al.* 2010; Gotoh and Khayyer 2016). Apart from deficiencies pertaining to the pressure accuracy and volume preservation, all the methods falling in the SPH family need excessive number of particles, even for sloshing in a tank, so that the computational cost will not be small at all (compared to the FEM for instance).

The method based on using exponential basis functions (EBFs) is among the element-free numerical methods (see Boroomand *et al.* 2010) that has so far been employed for the analysis of a wide range of engineering problems including those involving fluids with free surface movement. In this method, the general system's response is considered as a linear combination of exponential functions with complex exponents. The complex exponents are found such that the functions precisely satisfy the governing differential equations. The constant coefficients of the series are found by satisfying the boundary conditions on the set of boundary points.

Zandi *et al.* 2012a used the EBFs to solve some well-known benchmark fluid problems with free surface such as the water tank under harmonic forces, standing wave in a rectangular tank and the solitary wave. This method was also used for the analysis of incompressible stationary fluid flows in closed environments and also for the modeling of elasticity problems with fully incompressible materials (Zandi *et al.* 2012b). In the studies by Zandi *et al.* (2017) one may find one of the latest applications of the method in ocean engineering problems.

As can be traced in the literature, the method can be used either in a boundary node style or in a local form utilizing domain points. The local form of the exponential basis functions was developed by Mossaiby (2010). In this method, the solution area and the boundaries are discretized by a set of nodal points. The sensitivity of the accuracy of the responses to the irregular arrangement of points in the domain led to the provision of a new local method by Soleimanifar *et al.* (2014) which was applied to some common problems in physics and solid mechanics, such as Poisson and Helmholtz, elasticity problems and elastic wave on two-dimensional domains. The performance of the method has been investigated in solving the wave propagation and consolidation in saturated porous environments (Taghdirian 2011) and also in 3D simulation of nonlinear sloshing in tanks (Boroomand *et al.* 2016). The reader may refer to the studies by Shojaei *et al.* (2015) and (2016) for further extension of the method for some challenging problems.

In the studies conducted based on the use of EBFs presented for the analysis of engineering problems in recent years, the speed and accuracy of the meshless method as well as its low computational costs, compared to other methods, was demonstrated. In this article, it is attempted to analyze the fluid-structure interaction problems using the EBFs method combined with a Lagrangian approach for the fluid part.

In the fluid-structure interaction simulations presented in this paper it is assumed that the fluid is Newtonian inviscid fluid and the governing equation is written in Lagrangian description. The overall response of the fluid is considered as a linear combination of EBFs. The linear elastic structure, analyzed by the finite element method and Newmark time marching method, is subjected to the pressure induced by the fluid.

The main objective in this study is to show that a pressure based formulation using EBFs, previously presented in Zandi *et al.* 2012a, can be effectively

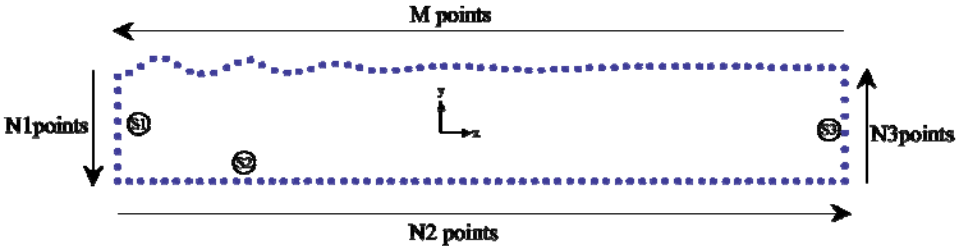

Fig. 1. Boundary points and the fluid coordinate system.

used in fluid-structure interaction. The capability of the EBFs in the modeling of relatively large sloshing, in tanks with rigid walls, has been demonstrated in our previous papers (e.g. see Zandi *et al.* 2012a). In order to show that the study is on a right path towards simulation of the fluid-structure interaction, one needs to study the movement of the structure due to non-linear behavior of the fluid. In this way we use a commercial program using the FEM for the validation and verification of the results. We shall discuss the time consumed and the pressure distribution found by both methods, i.e. the FEM and our method, to demonstrate the advantages of the proposed method.

This is the first study in its kind for using EBFs for the pressure for the aforementioned interaction problems especially when the free surface of the fluid undergoes nonlinear sloshing. The novel features of the study can be summarized as below:

- The presented method is a meshless one in a boundary node style. This domain reduction feature is expected to be more advantageous in 3D problems.
- It can be implemented in a code with a few lines.
- The use of pressure based formulation helps not only to directly relate the interface acceleration to the gradients of the pressure but also to directly evaluate the acting forces to the structure. Based on our previous experiments in using EBFs, it is expected that the pressure field be evaluated with high accuracy. This effect is highly appealing in fluid-structure interaction.
- The use of EBFs helps to find a solution which exactly satisfies the incompressibility condition with absolutely no approximation. This prominent feature of the formulation has a direct effect on the accuracy of the pressure field mentioned previously.

The boundary node method is simple to implement and, as can be seen later, it proves to be practically faster than the FEM methods used in commercial codes for the simulation of these interaction problems.

The layout of the paper is as follows; in section 2 the model problem and the core of the formulation is presented. Section 3 has been devoted to the validation of the formulation and presentation of the results. The overall conclusions are given in Section 4.

2. THE MODEL AND FORMULATION

It is well-understood that the governing equations (Navier-Stokes equations) of an inviscid incompressible fluid in Lagrangian description consist of the pressure gradients and the material acceleration terms and can be summarized as:

$$\rho_f \frac{D\dot{\mathbf{U}}_f}{Dt} = \nabla p + \rho_f \mathbf{g}\ ,\quad \mathbf{g} = \begin{Bmatrix} 0 \\ -g \end{Bmatrix} \tag{1}$$

by defining the pressure as the sum of two following parts:

$$p = p_H + \rho_f\, g\, y \tag{2}$$

the governing Eq. (1) reduces to:

$$\rho_f \frac{D\dot{\mathbf{U}}_f}{Dt} = \nabla p_H \tag{3}$$

In the above relations, the superscript f denotes the fluid, $\dot{\mathbf{U}}_f$ is the fluid velocity vector, ρ_f is the fluid density and g is the acceleration of gravity. p_H is the homogeneous part of the solution for the pressure (or hydrodynamic pressure) and $\rho_f\, g\, y$ is the particular part of the solution. The reader may note that such a split is always mathematically allowable since the gradient operator in Eqs. (1) and (3) is linear. Therefore, there is no restriction for the origin of the coordinate system, especially for the y axis. This means that the particular part of the solution in Eq. (2) plays the role of "semi-hydrostatic" pressure. This part of the solution may be interpreted as the true hydrostatic pressure when the origin of the y axis is considered at the (still) free surface. However, from a mathematical stand of view, this is not necessary and thus the origin of the coordinate system may be considered as a fixed point during the solution process (see Fig. 1). By applying divergence operator on both sides of Eq. (3) in a Lagrangian description (see Boroomand *et al.* 2016), and noting that $\nabla.\dot{\mathbf{U}}^f = 0$ due to the incompressibility effect, one may write:

$$\nabla.\dot{\mathbf{U}}_f = 0 \tag{4}$$

Note that Eq. (4) is valid for all instances of time. In order to solve the problem, a time marching approach should be adopted. To this end, the solution is performed within small time intervals as Δt. Although, no time variable is explicitly present in Eq. (4), the geometry of the fluid deforms as time goes on. The solution of Eq. (4) at each time step is considered as a series of exponential functions as:

$$\hat{p}_H = \sum_{i=1}^{l} c_i \, e^{\alpha_i x + \beta_i y} \tag{5}$$

The above equation may be written in a more compart form as:

$$\hat{p}_H = \boldsymbol{e}\,\boldsymbol{c} \tag{6}$$

Complex coefficients α_i and β_i in the exponent of the EBFs in Eq. (5) are found (see Appendix A) by direct insertion of the EBFs in Eq. (4). The unknown coefficients c_i, arranged in the vector $\boldsymbol{c}$, are found by imposition of the time-dependent boundary conditions. To this end, *N* boundary points are considered for the fluid boundaries from which *M* points are allocated to the fluid free surface while the remaining *N-M* points are considered on the boundaries labeled by number 1 to 3, associated with the bottom of the tank and the structure (surfaces S1 to S3 in Fig. 1).

Assuming that the solution has been found until time t^n, the fluid-structure geometry, the velocity and acceleration fields are available. With the geometry updated from the previous step, the pressure field can readily be reconstructed from the available boundary information. At the beginning of the time step *n*, i.e. $t^n \le t \le t^{n+1}$, based on the boundary conditions and the geometry which are already found at the end of the previous time step, the vectors $\overline{\mathbf{P}}_{\mathrm{B}}{}^n$ and $\overline{\mathbf{V}}_i^n$ are defined as follows:

$$\overline{\mathbf{P}}_{\mathrm{B}}{}^n = \begin{Bmatrix} \rho_f (n_x \ddot{u}_x + n_y \ddot{u}_y)\big|_{(x_1,y_1)^n} \\ \rho_f (n_x \ddot{u}_x + n_y \ddot{u}_y)\big|_{(x_2,y_2)^n} \\ \vdots \\ \rho_f (n_x \ddot{u}_x + n_y \ddot{u}_y)\big|_{(x_{N-M},y_{N-M})^n} \\ \hline -\rho_f g\, y^n_{N-M+1} \\ \vdots \\ -\rho_f g\, y^n_N \end{Bmatrix} \tag{7}$$

$$\overline{\mathbf{V}}_i^n = \begin{Bmatrix} (\alpha_i n_x + \beta_i n_y) e^{\alpha_i x + \beta_i y}\big|_{(x_1,y_1)^n} \\ \vdots \\ (\alpha_i n_x + \beta_i n_y) e^{\alpha_i x + \beta_i y}\big|_{(x_{N-M},y_{N-M})^n} \\ \hline e^{\alpha_i x + \beta_i y}\big|_{(x_{N-M+1},y_{N-M+1})^n} \\ \vdots \\ e^{\alpha_i x + \beta_i y}\big|_{(x_N,y_N)^n} \end{Bmatrix} \tag{8}$$

In Eqs. (7) and (8), $\mathbf{n} = \{n_x, n_y\}^T$ is the outward vector normal to the fluid boundaries while $\ddot{u}_x$ and $\ddot{u}_y$ are the components of the fluid acceleration. The *N-M* conditions above the dotted lines in the vectors $\overline{\mathbf{P}}_{\mathrm{B}}{}^n$ and $\overline{\mathbf{V}}_i^n$ pertain to the Neumann conditions collocated at boundaries S1 to S3 in Fig 1. These conditions are defined through the following relation at the three surfaces:

$$\rho\, \mathbf{n}^{\mathrm{T}} \ddot{\mathbf{U}} = \mathbf{n}^{\mathrm{T}} \nabla p_H \quad \Rightarrow \quad \left.\frac{\partial p_H}{\partial n}\right|_{\Gamma_s} = \rho\, \mathbf{n}^{\mathrm{T}} \ddot{\mathbf{U}}\big|_{\Gamma_s} \tag{9}$$

In Eq. (9), $\ddot{\mathbf{U}}\big|_{\Gamma_s}$ denotes the fluid's acceleration, at the interfaces of the fluid and structure (S1 to S3), which is to be considered equal to the structure's acceleration (also $\ddot{\mathbf{U}}\big|_{\Gamma_s}$ at S2 represents the ground acceleration).

The *M* conditions below the dotted lines in the vectors $\overline{\mathbf{P}}_{\mathrm{B}}{}^n$ and $\overline{\mathbf{V}}_i^n$ pertain to the Dirichlet conditions collocated at the free surface. These conditions are defined by setting the pressure to zero, at the free surface, which yields:

$$p_H\big|_{free} = -\rho_f\, g\, y\big|_{free} \tag{10}$$

In the above equation $(.)\big|_{free}$ denotes that the quantity is evaluated at the free surface. In order to make the solution independent of the dimensions and the coordinates of the solution area, and to achieve accurate results, the vector $\mathbf{V}_i^n$ is defined by normalizing the vector $\overline{\mathbf{V}}_i^n$ as:

$$\mathbf{V}_i^n = \frac{\overline{\mathbf{V}}_i^n}{S_i^n} \qquad S_i^n = \max_j\left(\left|\overline{V}_{i,j}^n\right|\right) \tag{11}$$

where $\overline{V}_{i,j}^n$ is the *j*th element of the vector $\overline{\mathbf{V}}_i^n$. Based on the definition of the vectors $\overline{\mathbf{P}}_{\mathrm{B}}{}^n$ and $\mathbf{V}_i^n$, and also by considering Eq. (6) one may write:

$$\mathbf{V}^{n}\,\boldsymbol{c}^{n} = \overline{\mathbf{P}}_{\mathrm{B}}^{\,n} \tag{12}$$

The vector of unknown coefficients $\boldsymbol{c}^{n}$ can now be calculated as follows:

$$\boldsymbol{c}^{n} = (\mathbf{V}^{n})^{+}\,\overline{\mathbf{P}}_{\mathrm{B}}^{\,n} \tag{13}$$

where $(.)^{+}$ indicates the pseudo-inverse of the matrix. By calculating the vector $\boldsymbol{c}^{n}$ one can evaluate the pressure at any point, either inside the domain or on its boundaries using Eqs. (6) and (2), including those which fall on the structure and fluid interface. The fluid pressure on the structure is calculated by inserting the coordinates of the nodal points of the structure's boundary as follows:

$$\hat{p}_{H}^{n} = \sum_{i=1}^{l} c_{i}^{n} e^{\alpha_i x+\beta_i y} = \mathbf{e}\,\mathbf{c}^{n} \tag{14}$$

Thus, the forces applied to the structure by the fluid may be calculated by the integration of the pressure on the elements having one edge at the interface:

$$\tilde{\mathbf{P}}_{\mathrm{int}}^{n} = \int_{\Gamma_{\mathrm{int}}} \mathbf{N}^{T}\,\hat{p}_{H}^{n}\,\mathrm{d}\Gamma + \rho_f\, g\,\boldsymbol{\eta}_{\mathrm{int}}\,\Gamma_{\mathrm{int}} \tag{15}$$

where, $\mathbf{N}$ is the matrix of the structural elements' shape functions, $\boldsymbol{\eta}_{\mathrm{int}}$ is the water height (from the still water depth) at the interface nodes and Γ_{int} is the interface of the elastic wall moving with fluid. By replacing the pressure with its equivalent in Eq. (14) the following equation is found:

$$\tilde{\mathbf{P}}_{\mathrm{int}}^{n} = \int_{\Gamma_{\mathrm{int}}} \mathbf{N}^{T}\mathbf{e}\,\mathbf{c}^{n}\mathrm{d}\Gamma + \rho_f\, g\,\boldsymbol{\eta}_{\mathrm{int}}\,\Gamma_{\mathrm{int}} = \mathbf{H}\mathbf{c}^{n} + \rho_f\, g\,\boldsymbol{\eta}_{\mathrm{int}}\,\Gamma_{\mathrm{int}} \tag{16}$$

where

$$\mathbf{H} = \int_{\Gamma_{\mathrm{int}}} \mathbf{N}^{T}\mathbf{e}\,\mathrm{d}\Gamma \tag{17}$$

By evaluating the forces applied on the interface, one may proceed to construct the vector of forces applied to the entire structure as follows:

$$\tilde{\mathbf{P}}^{n} = \begin{Bmatrix} \tilde{\mathbf{P}}_{\mathrm{int}}^{n} \\ \tilde{\mathbf{P}}_{rest}^{n} \end{Bmatrix} = \begin{Bmatrix} \tilde{\mathbf{P}}_{\mathrm{int}}^{n} \\ \mathbf{0} \end{Bmatrix} \tag{18}$$

In the above relation the subscript "*rest*" is used to indicate that the quantity is related to the nodes of the structure which are not on the interface (the rest of the structure). In case of the presence of an external force other than the fluid force, the elements of the vector $\tilde{\mathbf{P}}_{rest}^{n}$ can take on non-zero values. By forming the vector of forces applied to the entire structure, one may take into account the system of equations governing the structure:

$$\mathbf{M}\,\ddot{\mathbf{U}}_{S} + \mathbf{C}\,\dot{\mathbf{U}}_{S} + \mathbf{K}\,\mathbf{U}_{S} = \mathbf{P}(\mathrm{t}) \tag{19}$$

The system of equations is solved by Newmark method. In Eq. (19) the superscript S is used to indicate the structure part, $\mathbf{M}$ is the mass matrix, $\mathbf{C}$ is the damping matrix, $\mathbf{K}$ is the stiffness matrix, $\mathbf{P}(\mathrm{t})$ is the force vector and $\mathbf{U}$, $\dot{\mathbf{U}}$ and $\ddot{\mathbf{U}}$ are the displacement, velocity and acceleration vectors respectively.

Regarding the fact that only the boundary points' acceleration is required for the re-analysis of the fluid, by rewriting the Newmark algorithm for linear systems with multiple degrees of freedom, a simplified acceleration equation is achievable. To this end, one may first consider the increment of displacement, found from Newmark algorithm, as:

$$\Delta\mathbf{U}_{s}^{n} = \hat{\mathbf{K}}_{s}^{-1}\Delta\hat{\mathbf{P}}^{n} = \hat{\mathbf{K}}_{s}^{-1}\left\{\Delta\mathbf{P}^{n} + \mathbf{a}\,\dot{\mathbf{U}}_{s}^{n} + \mathbf{b}\,\ddot{\mathbf{U}}_{s}^{n}\right\} \tag{20}$$

where,

$$\hat{\mathbf{K}} = \mathbf{K} + \frac{\gamma_N}{\beta_N\,\Delta t}\mathbf{C} + \frac{1}{\beta_N\,(\Delta t)^{2}}\mathbf{M} \tag{21}$$

$$\mathbf{a} = \frac{1}{\beta_N\,\Delta t}\mathbf{M} + \frac{\gamma_N}{\beta}\mathbf{C} \tag{22}$$

and

$$\mathbf{b} = \frac{1}{2\beta_N}\mathbf{M} + \Delta t\,(\frac{\gamma_N}{2\beta_N} - 1)\,\mathbf{C} \tag{23}$$

In this research the Newmark parameters are considered as $\beta_N = 1/4$ and $\gamma_N = 1/2$.

By substituting $\Delta\mathbf{P}^{n}$, as the difference between the obtained forces in the time step n using the initial geometry and the forces applied on the structure at the end of step n, in Eq. (20) one may write:

$$\Delta\mathbf{U}_{s}^{n} = \hat{\mathbf{K}}_{s}^{-1}\left\{\left(\mathbf{P}^{n+1} - \tilde{\mathbf{P}}^{n}\right) + \mathbf{a}\,\dot{\mathbf{U}}_{s}^{n} + \mathbf{b}\,\ddot{\mathbf{U}}_{s}^{n}\right\} \tag{24}$$

On the other hand, considering the increment of the acceleration, the following relation is available from Newmark algorithm:

$$\ddot{\mathbf{U}}_{s}^{n+1} = \ddot{\mathbf{U}}_{s}^{n} + \Delta\ddot{\mathbf{U}}_{s}^{n} = \ddot{\mathbf{U}}_{s}^{n} + \frac{1}{\beta_N\,(\Delta t)^{2}}\Delta\mathbf{U}_{s}^{n} - \frac{1}{\beta_N\Delta t}\dot{\mathbf{U}}_{s}^{n} - \frac{1}{2\beta_N}\ddot{\mathbf{U}}_{s}^{n} \tag{25}$$

Finally, by substituting Eq. (24) in Eq. (25) the following relation may be written for the nodal accelerations of the structure:

$$\ddot{\mathbf{U}}_{s}^{n+1} = \ddot{\mathbf{U}}_{s}^{n} + \frac{1}{\beta_N\,(\Delta t)^{2}}\hat{\mathbf{K}}_{s}^{-1}\left\{\left(\mathbf{P}^{n+1} - \tilde{\mathbf{P}}^{n}\right) + \mathbf{a}\,\dot{\mathbf{U}}_{s}^{n} + \mathbf{b}\,\ddot{\mathbf{U}}_{s}^{n}\right\} - \frac{1}{\beta_N\Delta t}\dot{\mathbf{U}}_{s}^{n} - \frac{1}{2\beta_N}\ddot{\mathbf{U}}_{s}^{n} \tag{26}$$

To perform an analysis for the end of the time step, it is necessary to find the intermediate geometry and the associated acceleration field for the fluid. After calculating the coefficients c_i^{n} the acceleration field is found from the following equation:

$$\ddot{\mathbf{U}}_f^n = \frac{1}{\rho_f}\nabla \hat{p}_H^n = \sum_{i=1}^{I} \frac{c_i^n}{\rho_f} \begin{Bmatrix} \alpha_i \\ \beta_i \end{Bmatrix} e^{\alpha_i x^n + \beta_i y^n} \tag{27}$$

Now by the $\mathbf{U}_f^n$ and $\dot{\mathbf{U}}_f^n$ in hand, i.e. the displacement and velocity fields at the end of the previous time step, one may find an intermediate fluid geometry as follows:

$$\tilde{\mathbf{U}}_f^n = \mathbf{U}_f^n + \dot{\mathbf{U}}_f^n \Delta t + \frac{1}{2}\ddot{\mathbf{U}}_f^n \Delta t^2 \tag{28}$$

Such an intermediate geometry is used for the calculation of required vectors and matrices. Considering the boundary conditions of the intermediate geometry, one write:

$$\mathbf{V}^{n+1}\mathbf{c}^{n+1} = \overline{\mathbf{P}}_{\mathrm{B}}^{\,n+1} \tag{29}$$

The unknown vector $\mathbf{c}^{n+1}$ can again be calculated using the following equation:

$$\mathbf{c}^{n+1} = \mathbf{Q}^{n+1}\,\overline{\mathbf{P}}_{\mathrm{B}}^{\,n+1} \quad , \quad \mathbf{Q}^{n+1} = (\mathbf{V}^{n+1})^{+} \tag{30}$$

Note that $\overline{\mathbf{P}}_{\mathrm{B}}^{\,n+1}$ contains all nodal information for the fluid (at all boundaries as depicted in Fig. 1). The matrix $\mathbf{Q}^{n+1}$ and the array $\overline{\mathbf{P}}_{\mathrm{B}}^{\,n+1}$ each may be partitioned to two parts, one pertaining to the interface nodes and the other pertaining to the rest of the nodes at other boundaries:

$$\mathbf{c}^{n+1} = \mathbf{Q}^{n+1}\,\overline{\mathbf{P}}_{B}^{\,n+1} = \mathbf{Q}_1^{n+1}\,\overline{\mathbf{P}}_{B,\mathrm{int}}^{\,n+1} + \mathbf{Q}_2^{n+1}\,\overline{\mathbf{P}}_{B,comp}^{\,n+1} \tag{31}$$

In the above equation $\overline{\mathbf{P}}_{B,n+1}^{\mathrm{int}}$ is an array associated with the fluid boundary conditions at the interface nodes that is calculated through the structural acceleration $\ddot{\mathbf{U}}_s^{n+1}$:

$$\overline{\mathbf{P}}_{B,\mathrm{int}}^{\,n+1} = \rho_f\, \boldsymbol{n}^T \mathbf{A}\, \ddot{\mathbf{U}}_{s,\mathrm{int}}^{n+1} \tag{32}$$

In this equation $\boldsymbol{n}$ is the unit vector normal to the fluid boundary at the interface. $\mathbf{A}$ is a matrix relating the structural nodal accelerations to the fluid pressure nodes (see Appendix B). $\overline{\mathbf{P}}_{B,comp}^{\,n+1}$ is the complementary part of the boundary conditions (in the fixed and the free boundaries) which is defined as follows (based on the zero values for the pressure at the free surface and the acceleration at the fixed boundary):

$$\overline{\mathbf{P}}_{B,comp}^{\,n+1} = \begin{Bmatrix} \mathbf{0} \\ - - - - - \\ -\rho_f\, g\, \tilde{y}_{N-M+1}^{\,n+1} \\ \vdots \\ -\rho_f\, g\, \tilde{y}_N^{\,n+1} \end{Bmatrix} \tag{33}$$

By substituting Eq. (32) in Eq. (31) the vector $\mathbf{c}^{n+1}$ is defined as follows:

$$\mathbf{c}^{n+1} = \mathbf{Q}_1^{n+1}\,\rho_f\, \boldsymbol{n}^T \mathbf{A}\, \ddot{\mathbf{U}}_{s,\mathrm{int}}^{n+1} + \mathbf{Q}_2^{n+1}\,\overline{\mathbf{P}}_{B,comp}^{\,n+1} \tag{34}$$

In the above equation the array $\ddot{\mathbf{U}}_{s,\mathrm{int}}^{n+1}$ contains all unknown nodal accelerations on the interface. By substituting the new definition of $\mathbf{c}^{n+1}$ in Eq. (16), the forces applied to the structure can now be calculated by the following equation:

$$\mathbf{P}_{\mathrm{int}}^{n+1} = \mathbf{H}\left(\mathbf{Q}_1^{n+1}\rho_f \boldsymbol{n}^T \mathbf{A}\, \ddot{\mathbf{U}}_{s,\mathrm{int}}^{n+1} + \mathbf{Q}_2^{n+1}\,\overline{\mathbf{P}}_{B,comp}^{\,n+1}\right) + \rho_f\, g\, \boldsymbol{\eta}_{\mathrm{int}} \Gamma_{\mathrm{int}} \tag{35}$$

As a result, the vector of the whole structure's forces is arranged as follows:

$$\mathbf{P}^{n+1} = \begin{Bmatrix} \mathbf{P}_{\mathrm{int}}^{n+1} \\ \mathbf{P}_{rest}^{n+1} \end{Bmatrix} = \begin{Bmatrix} \mathbf{H}\left(\mathbf{Q}_1^{n+1}\rho_f \boldsymbol{n}^T \mathbf{A}\, \ddot{\mathbf{U}}_{s,\mathrm{int}}^{n+1} + \mathbf{Q}_2^{n+1}\overline{\mathbf{P}}_{B,comp}^{\,n+1}\right) + \rho_f\, g\, \boldsymbol{\eta}_{\mathrm{int}} \Gamma_{\mathrm{int}} \\ \mathbf{P}_{rest}^{n+1} \end{Bmatrix} =$$
$$\begin{Bmatrix} \mathbf{H}\left(\mathbf{Q}_1^{n+1}\rho_f \boldsymbol{n}^T \mathbf{A}\, \ddot{\mathbf{U}}_{s,\mathrm{int}}^{n+1}\right) \\ \mathbf{0} \end{Bmatrix} + \begin{Bmatrix} \mathbf{H}\left(\mathbf{Q}_2^{n+1}\overline{\mathbf{P}}_{B,comp}^{\,n+1}\right) + \rho_f\, g\, \boldsymbol{\eta}_{\mathrm{int}} \Gamma_{\mathrm{int}} \\ \mathbf{0} \end{Bmatrix} \tag{36}$$

By substituting such an array of forces in Eq. (26) one may write:

$$\ddot{\mathbf{U}}_s^{n+1} - \frac{1}{\beta_N (\Delta t)^2}\hat{\mathbf{K}}_s^{-1}\left(\begin{Bmatrix} \mathbf{H}\left(\mathbf{Q}_1^{n+1}\rho_f \boldsymbol{n}^T \mathbf{A}\, \ddot{\mathbf{U}}_{s,\mathrm{int}}^{n+1}\right) \\ \mathbf{0} \end{Bmatrix} + \begin{Bmatrix} \mathbf{H}\left(\mathbf{Q}_2^{n+1}\overline{\mathbf{P}}_{B,comp}^{\,n+1}\right) + \rho_f\, g\, \boldsymbol{\eta}_{\mathrm{int}} \Gamma_{\mathrm{int}} \\ \mathbf{0} \end{Bmatrix}\right) =$$
$$\frac{1}{\beta_N (\Delta t)^2}\hat{\mathbf{K}}_s^{-1}\left\{-\tilde{\mathbf{P}}^n + \mathbf{a}\,\dot{\mathbf{U}}_s^n + \mathbf{b}\,\ddot{\mathbf{U}}_s^n\right\} - \frac{1}{\beta_N \Delta t}\dot{\mathbf{U}}_s^n + (1 - \frac{1}{2\beta_N})\ddot{\mathbf{U}}_s^n \tag{37}$$

or

$$\overline{\mathbf{M}}\ddot{\mathbf{U}}_s^{n+1} = \frac{1}{\beta_N (\Delta t)^2}\hat{\mathbf{K}}_s^{-1}\left\{-\tilde{\mathbf{P}}^n + \mathbf{a}\,\dot{\mathbf{U}}_s^n + \mathbf{b}\,\ddot{\mathbf{U}}_s^n\right\} - \frac{1}{\beta_N \Delta t}\dot{\mathbf{U}}_s^n + (1 - \frac{1}{2\beta_N})\ddot{\mathbf{U}}_s^n + \frac{1}{\beta_N (\Delta t)^2}\hat{\mathbf{K}}_s^{-1}\begin{Bmatrix} \mathbf{H}\left(\mathbf{Q}_2^{n+1}\overline{\mathbf{P}}_{B,comp}^{\,n+1}\right) + \rho_f\, g\, \boldsymbol{\eta}_{\mathrm{int}} \Gamma_{\mathrm{int}} \\ \mathbf{0} \end{Bmatrix} \tag{38}$$

In this equation $\overline{\mathbf{M}}$ is defined as follows:

$$\overline{\mathbf{M}} = \mathbf{I} - \frac{1}{\beta_N (\Delta t)^2}\hat{\mathbf{K}}_s^{-1}\begin{bmatrix} \mathbf{H}\left(\mathbf{Q}_1^{n+1}\rho_f \boldsymbol{n}^T \mathbf{A}\right) & \mathbf{0} \\ \mathbf{0} & \mathbf{0} \end{bmatrix} \tag{39}$$

Finally the nodal accelerations of the structure are calculated from Eq. (38) as:

$$\ddot{\mathbf{U}}_s^{n+1} = \overline{\mathbf{M}}^{-1}\left\{\frac{1}{\beta_N(\Delta t)^2}\hat{\mathbf{K}}_s^{-1}\left\{-\tilde{\mathbf{P}}^n + \mathbf{a}.\dot{\mathbf{U}}_s^n + \mathbf{b}.\ddot{\mathbf{U}}_s^n\right\} - \frac{1}{\beta_N\Delta t}\dot{\mathbf{U}}_s^n + (1-\frac{1}{2\beta_N})\ddot{\mathbf{U}}_s^n + \frac{1}{\beta_N(\Delta t)^2}\hat{\mathbf{K}}_s^{-1}\begin{Bmatrix}\mathbf{H}\left(\mathbf{Q}_2^{n+1}\overline{\mathbf{P}}_{B,comp}^{n+1}\right) + \rho_f g\,\boldsymbol{\eta}_{\text{int}}\Gamma_{\text{int}}\\ \mathbf{0}\end{Bmatrix}\right\} \tag{40}$$

By calculating $\ddot{\mathbf{U}}_s^{n+1}$ and substituting it in the definition of $\mathbf{c}^{n+1}$ in Eq. (34), the solution of the coupled system at the end of the time step is completed. With the solution at the end of time step in hand, it is necessary to calculate the values required to continue the solution in the next step. Assuming linear acceleration, the nodal velocities and displacements of the structure are obtained by the nodal accelerations obtained at the end of the steps $n-1$ and n:

$$\dot{\mathbf{U}}_s^{n+1} = \dot{\mathbf{U}}_s^n + \frac{1}{2}\left(\ddot{\mathbf{U}}_s^{n+1} + \ddot{\mathbf{U}}_s^n\right)\Delta t \tag{41}$$

$$\mathbf{U}_s^{n+1} = \mathbf{U}_s^n + \dot{\mathbf{U}}_s^n\Delta t + \left(\frac{\ddot{\mathbf{U}}_s^{n+1}}{6} + \frac{\ddot{\mathbf{U}}_s^n}{3}\right)\Delta t^2 \tag{42}$$

Acceleration field of the fluid in the intermediate geometry is obtained by the following equation:

$$\ddot{\tilde{\mathbf{U}}}_f^{n+1} = \sum_{i=1}^{l}\frac{c_i^{n+1}}{\rho}\begin{Bmatrix}\alpha_i\\ \beta_i\end{Bmatrix} e^{\alpha_i\ddot{x}^{n+1}+\beta_i\ddot{y}^{n+1}} \tag{43}$$

Now the new fluid's velocity field and its geometry as the initial boundary conditions of the next step are calculable based on the acceleration obtained at the beginning of the step, the intermediate geometry accelerations, and also the velocities and displacements at the end of the time step $n-1$:

$$\dot{\mathbf{U}}_f^{n+1} = \dot{\mathbf{U}}_f^n + \frac{1}{2}\left(\ddot{\tilde{\mathbf{U}}}_f^{n+1} + \ddot{\mathbf{U}}_f^n\right)\Delta t \tag{44}$$

$$\mathbf{U}_f^{n+1} = \mathbf{U}_f^n + \dot{\mathbf{U}}_f^n\Delta t + \left(\frac{\ddot{\tilde{\mathbf{U}}}_f^{n+1}}{6} + \frac{\ddot{\mathbf{U}}_f^n}{3}\right)\Delta t^2 \otimes \tag{45}$$

In the next section we shall present the results of some numerical experiments using the proposed formulation.

3. NUMERICAL EXPERIMENTS

In the forthcoming simulations, the validation and verification of the formulation are performed through comparison of the results with those of the FEM implemented in a commercial code. To this end, after definition of the problem, we shall first compare the results found for nonlinear sloshing in a tank with rigid walls for which some analytical solutions are available. This helps to estimate the errors, for the liquid part, for the two methods which may be used for finding an appropriate mesh resolution for the FEM and also an appropriate number of nodes in our formulation so that a fair comparison can be performed when fluid-structure interaction is of concern.

3.1 Definition of the Problem

In this example a square tank with the length of $l = 1m$ filled with water, with the density of $\rho = 1000\,kg/m^3$, is considered. The left wall of the tank is made of steel material with $\nu = 0.3$, $\rho = 7860\,kg/m^3$ and $E = 198\times10^9\,Pa$ (see Fig. 2).

The tank is fixed at the base while its right wall is considered rigid. The fluctuation of the fluid and the elastic wall are affected by a standing wave. The initial condition of the fluid is specified as follows:

$$\eta(x) = A_f\cos\left(k\left(x + l/2\right)\right) \tag{46}$$

where, $\eta(x)$ is the height of the wave from the still water level, A_f is the amplitude of the initial wave profile, $k = 2\pi/\lambda$ while λ is the wavelength. The subscript f denotes the fluid part. The initial fluid free surface is defined as a cosine wave with an amplitude of $A_f = 0.005m$ considering $\lambda = l/2$ while the water height in the standing condition is $h = 1m$.

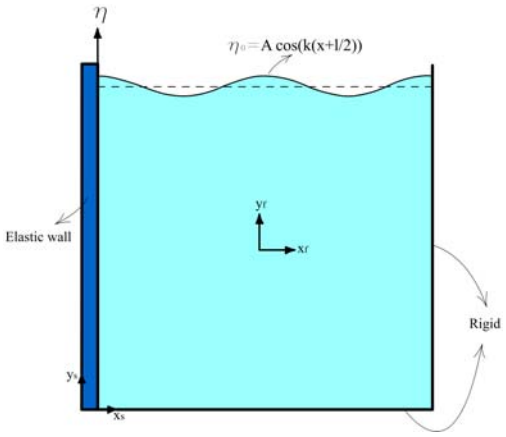

Fig. 2. Initial conditions of the standing wave in the tank with the elastic wall (S and f denote the structure and fluid, respectively).

This example is modeled by a computer code, developed by the authors, in the programming environment of Mathematica (Wolfram Mathematica 9.0 in 2012) for the simulation of fluid-structure interaction problems and also by a commercial code using the finite element method (i.e. the Abaqus software). In the next section, further details of the two types of modeling are given.

3.2 Details of the Proposed Modelling

In the proposed model, as mentioned earlier, the elastic wall section is analyzed by the finite element

formulation while the fluid part is simulated using EBFs. The fluid boundaries are discretized by 206 boundary points (Fig. 3) from which 51 points are allocated to each side, including the elastic wall, while 104 points are allocated to upper and lower boundaries, including the free surface.

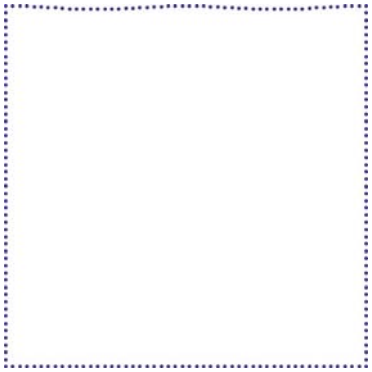

Fig. 3. Initial configuration of fluid boundary points in EBFs method.

The size of the wall is considered as 0.05 *m*×1.01 *m* (the height of the elastic wall is larger than the initial left water level). The wall is discretized by 9-node elements (only one element used through the thickness). Up to the height of 0.995, the wall is discretized by 10 elements ($1-A_f = 1-0.005 = 0.995$) while 6 elements are used to discretize the rest of the wall, i.e. the part with the height of $2A_f$ on which the water level is expected to fluctuate (Fig. 4).

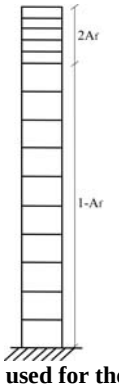

Fig. 4. Elements used for the elastic wall in Mathematica.

Damping matrix factors are calculated based on the first and second frequencies of the wall (without water), evaluated as $\omega_1 = 234.954$, $\omega_2 = 1456.96$, and considering the damping ratio of $\xi = 0.05$ while using the Rayleigh's damping relations (Chopra 1995). Therefore the damping matrix $\mathbf{C}$ is assumed as follows:

$$\mathbf{C} = \alpha_c \mathbf{M} + \beta_c \mathbf{K}, \alpha_c = 20.2326, \beta_c = 5.9 \times 10^{-5} \quad (47)$$

In this equation $\mathbf{K}$ is the stiffness matrix and $\mathbf{M}$ is the mass matrix. In order to study the fluid–structure interaction, the wall vibration due to the hydrodynamic pressure is investigated. To this end, the effect of hydrostatic pressure is removed from the solution by applying a static pressure on the wall.

3.3 Details of the Modeling in Abaqus

In the FEM model, the geometry of the fluid part is considered similar to that described in the previous section (Abaqus 6.11 in 2011). The fluid is defined as Newtonian with the viscosity of 10^{-9} *Pa.s* and the speed of sound as $v = 1483\, m/s$. The analyses are performed with two sets of damping coefficients $\alpha_c = 20.2326$ and $\alpha_c = 202.326$ (while $\beta_c = 0$ for both cases). It is noteworthy that using a non-zero value for β_c in Abaqus software greatly increases the CPU time, especially when fluid-structure interaction is involved (e.g. for a 5 second solution and using 4096 elements, the CPU time is about 33 hours and 20 minutes for $\beta = 0$ while it takes 186 days for $\beta_c = 5.9 \times 10^{-5}$). Therefore in the modeling β_c is considered zero. The option of "explicit dynamic solution" in the software was used in the interaction analysis and the solution's stages are defined in one step.

As mentioned in the previous section, since the objective here is to study the problem under hydrodynamic forces, the effect of water hydrostatic pressure (or the initial deformation of the elastic structure caused by the hydrostatic pressure) is removed by considering a hydrostatic pressure through the software's feature of "Load/Tools/AnalyticalField/Manager" and defining an equation as $9845y - 9845$ (see Fig. 5 for the distribution and also Fig. 2 for the origin of y).

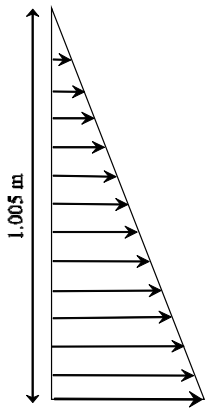

Fig. 5. Distribution of the hydrostatic pressure on the inside edge of the elastic wall.

Based on the problem type and the features of the software, the discretization of the fluid and elastic wall is performed by 4-node plane strain elements

Table 1 Sensitivity of the numerical solution for a tank with rigid walls

Method	Property		Error of Period (%)	Error of Amplitude (%)	Total CPU Time (min)
	Elements or boundary nodes	Δt (sec)			
Abaqus	169 elements	0.025	19.88	102.42	3
	1024 elements	0.025	3.14	31.2	33
	2500 elements	0.025	2.14	26	120
	4096 elements	0.025	0.49	14.2	240
EBFs	206 boundary node	0.025	0.49	25.7	40
		0.01	0.48	9.56	100

and the discretization of the rigid parts is performed by linear 2-node elements. The number of square elements used in the discretization of the fluid is 4096 and the elastic structure is discretized by 198 elements (Fig. 6).

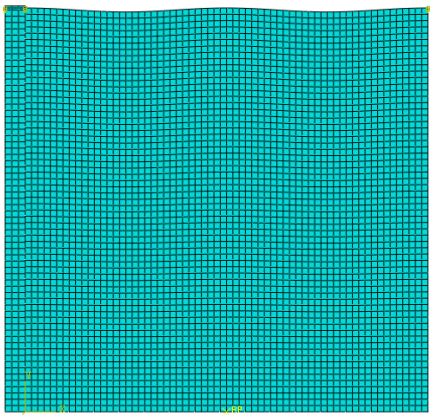

Fig. 6. Initial form of discretization of the fluid and structure in ABAQUS software.

3.4 Results for Rigid Tank

In order to find the best element size for the fluid part, the problem is first solved for the case in which all walls are rigid. Such a case has an analytical solution presented by Faltinsen (1974). Therefore by comparing the numerical solutions, found form either Abaqus or the EBFs, with the analytical one an appropriate element size in Abaqus, whose results is comparable with that of the EBFs, may be found and thus comparison of the two methods, in the solution of the tank with elastic wall, will then be possible. To this end, the water fluctuation at the walls of the tank is evaluated with different number of elements, i.e. 169, 1024, 2500 and 4096 elements. The time increment is taken as $\Delta t = 0.025\,\text{sec}$. The computed errors and the CPU times are presented in Table 1. We have included the results of EBFs with $\Delta t = 0.01\,\text{sec}$. As can be observed in Table 1, to reach a rather similar acceptable accuracy in both methods, 4096 elements are required in the discretization of fluid part in the FE analysis in Abaqus. Thus using the same number of elements for the elastic reservoir may lead to a fair comparison between the two methods. The reader may note that the accuracy of the results with 2500 elements and $\Delta t = 0.025\text{sec}$ is rather similar to the accuracy of the results obtained by EBFs with the same time increment. However, the errors calculated are not acceptable from a computational stand of view. An important feature reported in the table is the CPU time of the solutions (the CPU used in this paper is 2.27 GHz Core i5). It can be seen that for results with rather similar accuracies, the CPU time of EBFs is much less than the CPU time of the FEM (or vice versa, for results with rather similar CPU times, the error of EBFs' results is considerably less than the errors of the FEM's results).

3.5 Results for Fluid-Structure Interaction

In this section the results found for elastic tank are presented. Here the objective is not only verification of the results but also demonstration of the advantages of the proposed method over the existing tools. Figure. 7 illustrates the fluctuation of water at the top left node of the fluid versus time found from both EBFs and Abaqus software. The time increment in the EBFs solution is taken as $\Delta t = 0.005\,\text{sec}$ and in Abaqus the increment of time is $\Delta t = 0.01\,\text{sec}$. Note that due to the presence of an elastic wall in the solution, the time increments in both methods are taken less than those used for the tank with rigid walls (other solution characteristics in both methods are similar to those presented in Table 1, i.e. 4096 elements in FEM and 206 boundary nodes in EBFs). The analyses are performed using $\alpha_c = 20.2326$ and $\beta_c = 0$ (see Eq. (47)).

As it can be observed, the results of the two methods are in good agreement in terms of period and amplitude.

In Figs. 8 and 9, the variation of hydrodynamic pressure at the interface between the fluid and elastic wall along the wall's height is presented at the times $t = 1.42$ (minimum water height in the third phase) and $t = 1.71$ (maximum water height at the end of the third phase). As it can be observed from the figures, the hydrodynamic pressure found from Abaqus exhibits some unrealistic fluctuations

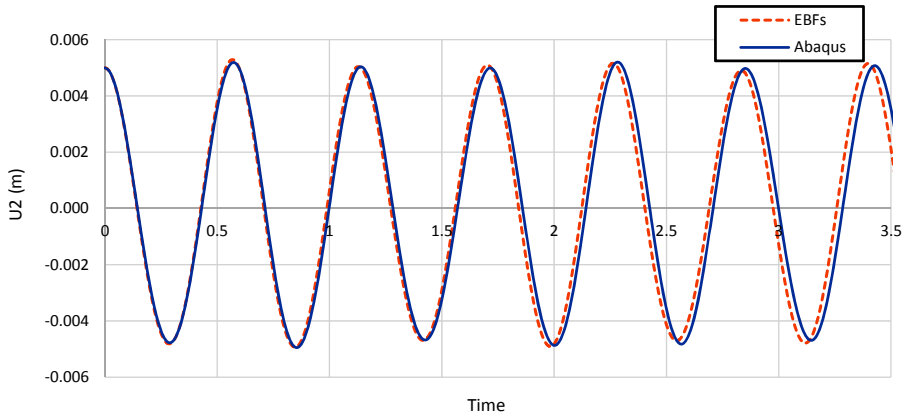

Fig. 7. Comparison of the calculated wave heights at the left node of the fluid on the interface with elastic structure.

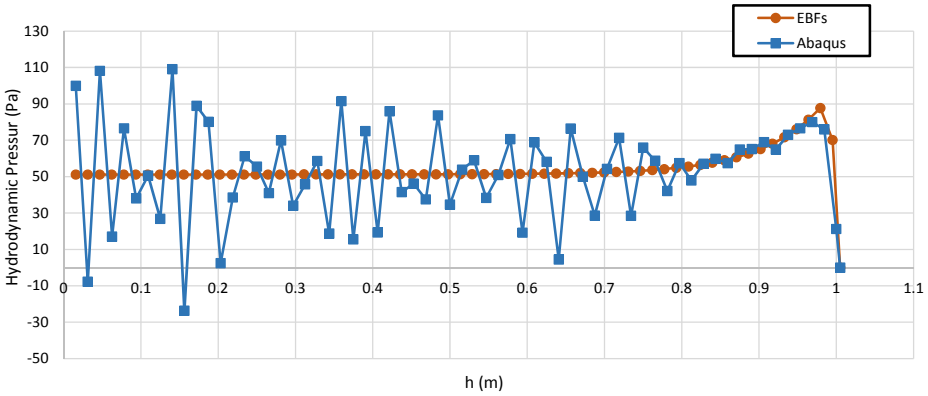

Fig. 8. Hydrostatic pressure distribution on the elastic wall at $t = 1.42$.

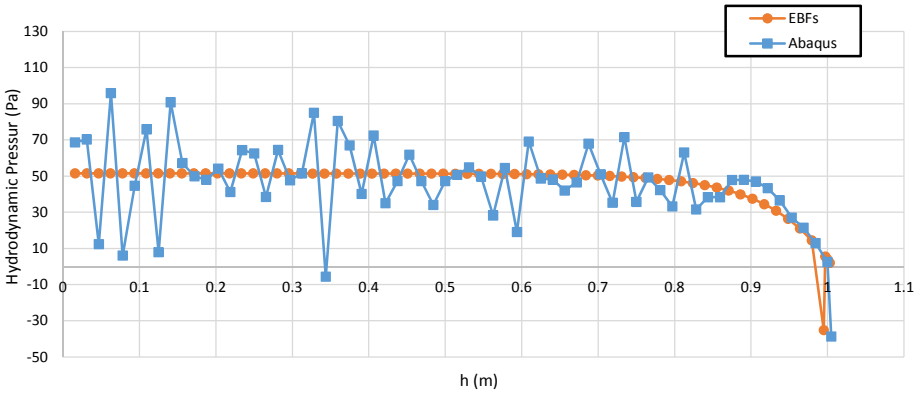

Fig. 9. Hydrostatic pressure distribution on the elastic wall at $t = 1.71$

and this effect is in contrast with the results of EBFs solution. It appears that the pressure found from Abaqus fluctuates around the EBFs results. This effect clearly shows that the EBFs results may be considered more reliable while the computational effort is much less than that of the FEA. Using similar CPU for both analyses, the solution in Abaqus software takes 33 hours and 20 minutes while the solution using EBFs takes 4 hours and 20 minutes (noting that, unlike the Abaqus software, the code written for the EBFs has not been professionally optimized). This clearly shows the advantage of using the proposed meshless method in the solution of fluid-structure interaction problems.

Figure 10a shows the variation of horizontal displacement of the top of the elastic wall on interface with fluid (h=1.005 m) obtained from EBFs method and Abaqus software. As can be observed in this figure, the period and amplitude of the oscillation found from both methods are in excellent agreement. Some additional oscillations are observable within the period of

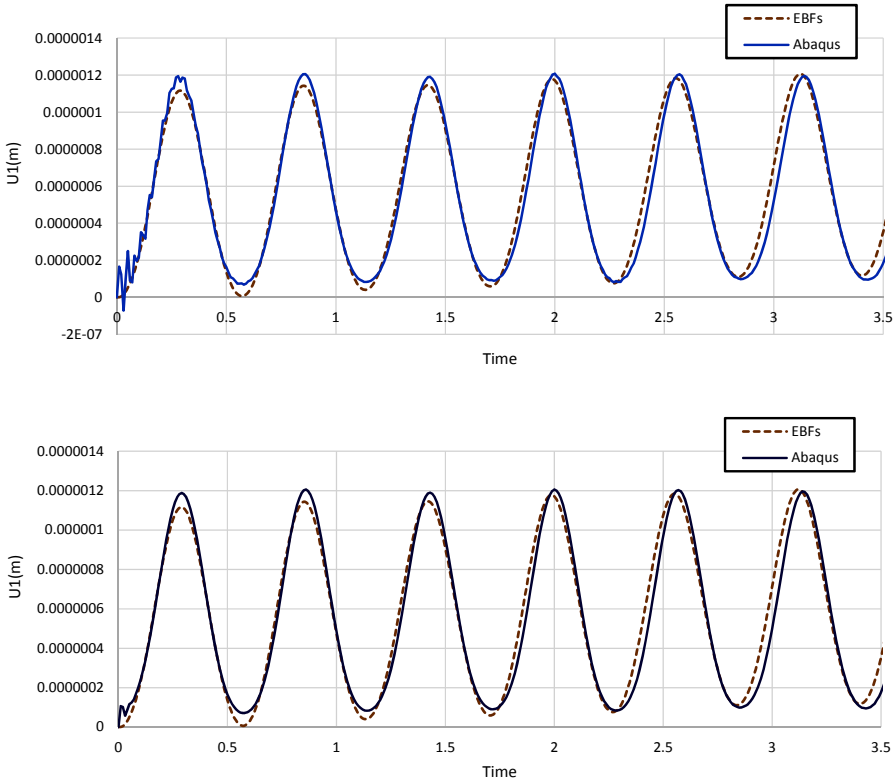

(a)

(b)

Fig. 10. Comparison of the horizontal displacement of the top point of the elastic wall on the interface with fluid (h=1.005 m); (a) for α_c = 20.2326 , (b) for α_c = 202.326

$0 \le t \le 0.25$sec which decay as the time goes on. This additional wall vibration may be attributed to the free vibration of the wall. In order to provide better insight to the problem, the solutions have then been repeated using higher damping coefficient α_c = 202.326 . The results are presented in Fig. 10b. It can clearly be seen that while the oscillation in the Abaqus results is reduced and damped fast, no meaningful change is perceivable for the overall wall behavior.

4. CONCLUSIONS

In this paper a boundary node method, suitable for the simulation of interaction between inviscid-incompressible fluids with their containers, has been proposed. It has been also shown that the use of pressure based formulation helps not only to directly relate the interface acceleration to the gradients of the pressure but also to directly evaluate the acting forces to the structure.

Apart from the features as: domain reduction, simplicity of the implementation and capability of exactly satisfying the incompressibility condition; the following advantages have been experienced during the numerical experiments:

- It is considerably faster than the FEM methods, e.g. those used in commercial codes. The reduction in computational cost has been evaluated as (at least) one-eighth of the Abaqus software, considering that the program used in this research has not been optimized, in contrast to some well-known professional and commercial codes such as Abaqus. This feature may become more advantageous while dealing with 3D problems in which domain reduction is of more importance.
- It results in a meaningful/accurate pressure distribution compared to the pressure found by the FEM.

Since the formulation of the proposed method is based on using smooth bases, it cannot be directly applied to modelling of breaking waves in the tanks (which involve singularities in the solution). Appropriate singular bases may be introduced to the solution, as suggested by Mossaiby *et al.* (2015). There is a possibility of constructing the singular bases for special cases (see for instance Noormohammadi and Boroomand 2017). These issues are currently under consideration.

APPENDIX A

By placing $\hat{p}_H$ in Eq. (5), the relationship between complex values α_i and β_i are obtained as follow:

$$\alpha_i^2 + \beta_i^2 = 0 \Rightarrow \begin{cases} \alpha_i = \pm \mathbf{i}\, \beta_i \\ \beta_i = \pm \mathbf{i}\, \alpha_i \end{cases} \qquad \text{(A-1)}$$

In this equation $\mathbf{i}=\sqrt{-1}$ is a unique imaginary number. Therefore by choosing the factors α_i and β_i the differential equations are satisfied in all areas. These factors are chosen according the following pattern which was initially given by Boroomand *et al*. (2010):

$$\begin{cases}\alpha_i=\pm G\gamma\left(\frac{j}{n}+2\mathbf{i}\right)\\ \beta_i=\pm G\gamma\left(\frac{j}{n}+2\mathbf{i}\right)\end{cases} \tag{A-2}$$

where

$$\begin{cases}G=1,2,...,m & 4<m\\ j=1,2,...,n & 2<n<8\end{cases} \tag{A-3}$$

The following equation is proposed for γ

$$\gamma=\frac{\kappa}{Max(L_X,L_Y)} \qquad 3.5\le\kappa\le 4.5 \tag{A-4}$$

where, L_X and L_Y are the dimensions of the rectangle that circumscribes the domain. In this study m and n are considered as 10 and 5 respectively and 4 is the value proposed for κ; therefore, $l=8m\ n=400$ exponential bases are defined.

APPENDIX B

The matrix A relates the fluid and structure nodes in common boundary:

$$\ddot{\mathbf{U}}_{f,\text{int}}=\mathbf{A}\ddot{\mathbf{U}}_{s,\text{int}} \tag{B -1}$$

Assuming that the normal vector of the interface between the structure and the fluid is in x coordinate and linearly acceleration between two successive nodes of the structure at the common boundary, the corresponding elements of acceleration $\ddot{\mathbf{U}}_x$ of matrix **A** are formed as follows:

If $\quad \mathrm{y}_s^k<\mathrm{y}_f^j\le\mathrm{y}_s^{k+1}$

$$A_{jk}=\frac{\mathrm{y}_f^j-\mathrm{y}_s^k}{\mathrm{y}_s^{k+1}-\mathrm{y}_s^k}$$

$$A_{jk+1}=\frac{\mathrm{y}_s^{k+1}-\mathrm{y}_f^j}{\mathrm{y}_s^{k+1}-\mathrm{y}_s^k}$$

Else

$$A_{jk}=0 \tag{B-2}$$

In this equation the superscripts f and s denote the fluid and the structure, respectively. It should be noted that due to the lack of transferring the acceleration along the y axis (tangential level) between the structure and fluid, in the rows and columns corresponding to the $\ddot{\mathbf{U}}_y$ the value 0 is placed in matrix **A**.

REFERENCES

Abaqus 6.11 (2011). Getting Started with Abaqus: Interactive Edition, 10.6 Hyperelasticity.

Antoci, C., M. Gallati and S. Sibilla (2007). Numerical simulation of fluid–structure interaction by SPH. *Computers and Structures* 85, 879–890.

Boroomand, B., S. Bazazzadeh and S. M. Zandi (2016). On the use of Laplace's equation for pressure and a mesh-free method for 3D simulation of nonlinear sloshing in tanks. *Ocean Engineering* 122, 54-67.

Boroomand, B., S. Soghrati and B. Movahedian (2010). Exponential basis functions in solution of static and time harmonic elastic problems in a meshless style. *International Journal for Numerical Methods in Engineering* 81, 971–1018.

Chopra, A. K. (1995). *Dynamics of structures, Theory and applications of earthquake engineering*, Prentice-Hall, New Jersey.

Faltinsen, O. (1974). A nonlinear theory of sloshing in rectangular tanks. *Journal of Ship Research* 18(4), 224–241.

Firouz-Abadi, R. D., H. Haddadpour and M. Ghasemi (2009). Reduced order modeling of liquid sloshing in 3D tanks using boundary element method. *Engineering Analysis with Boundary Elements* 33, 750–761.

Gotoh, H. and A. Khayyer (2016). Current achievements and future perspectives for projection-based particle methods with applications in ocean engineering. *Journal of Ocean Engineering and Marine Energy* 2(3), 251–278.

Idelsohn, S. R., J. Marti, P. Becker and E. Oñate (2014). Analysis of multifluid flows with large time steps using the particle finite element method. *International Journal for Numerical Methods in Fluid* 75, 621-644.

Kolaei, A., S. Rakheja and M. J. Richard (2015). A coupled multimodal and boundary-element method for analysis of anti-slosh effectiveness of partial baffles in a partly-filled container. *Computers & Fluids* 107, 43–58.

Lee, E. S., D. Violeau, R. Issa and S. Ploix (2010). Application of weakly compressible and truly incompressible SPH to 3-D water collapse in waterworks. *Journal of Hydraulic Research* 48, 50–60.

Liu, X., P. Lin and S. Shao (2014). An ISPH simulation of coupled structure interaction with free surface flows. *Journal of Fluids and Structures* 48, 46-61.

Liu, X., S. Shao, P. Lin and S. Tan (2016). 2D Numerical ISPH wave tank FOR complex fluid-structure coupling problems. *International Journal of Offshore and Polar*

Engineering 26, 26-32.

Lucy, L .B. (1977). A numerical approach to the testing of the fission hypothesis. *Astronomical Journal* 82, 1013–1024.

Ma, Q. W. (2005). Meshless local Petrov–Galerkin method for two-dimensional nonlinear water wave problems. *Journal of Computational Physics* 205, 611-625.

Mayrhofer, A., M. Ferrand, C. Kassiotis, D. Violeau and F. X. More (2015). Unified semi-analytical wall boundary conditions in SPH: analytical extension to 3-D. *Numerical Algorithms* 68(1), 15–34.

Monaghan, J. J. (1994). Simulating free surface flows with SPH, *Journal of Computational Physics* 110, 399–406.

Mossaiby, F. (2010). *Solution of Solid Mechanics' Problems in Bounded and Unbounded Domains Using Semi-Analytic and Finite Element Methods*. Ph.D. thesis, Isfahan University of Technology, Isfahan, Iran.

Mossaiby, F., M. Bazrpach and A. Shojaei (2015). Extending the method of exponential basis functions to problems with singularities. *Engineering Computations* 32, 406-423.

Nguyen-Thoi, T., P. Phung-Van, T. Rabczuk, H. Nguyen-Xuan and C. Le-Van (2013). An application of the ES-FEM in solid domain for dynamic analysis of fluid-solid interaction problems. *International Journal of Computational Methods* 10(1), 1340003 (26 pages).

Noormohammadi, N. and B. Boroomand (2017). Construction of equilibrated singular basis functions without a priori knowledge of analytical singularity order. *Computers and Mathematics with Applications* 73, 1611-1626.

Oñate, E., S. R. Idelsohn, F. Del Pin and R. Aubry (2004). The particle finite element method. an overview. *International Journal of Computational Methods* 1(2), 267–307.

Randles, P. W. and L. D. Libersky (1996). Smoothed particle hydrodynamics: some recent improvements and applications. *Computer Methods in Applied Mechanics and Engineering* 139. 375–408.

Ren, B., M. He, Y. Li and P. Dong (2017). Application of smoothed particle hydrodynamics for modeling the wave-moored floating breakwater interaction. *Applied Ocean Research* 67, 277–290.

Shojaei, A., B. Boroomand and E. Soleimanifar (2016). A meshless method for unbounded acoustic problems. *Journal of Acoustical Society of America* 139, 2613 – 2623.

Shojaei, A., B. Boroomand and F. Mossaiby (2015). A simple meshless method for challenging engineering problems. *Engineering Computations* 32, 1567 – 1600.

Soleimanifar, E., B. Boroomand and F. Mossaiby (2014). A meshless method using local exponential basis functions with weak continuity up to a desired order. *Computational Mechanics* 53(6), 1355-1374.

Sriram, V. and Q. W. Ma (2012). Improved MLPG_R method for simulating 2D interaction between violent waves and elastic structures. *Journal of Computational Physics* 231, 7650-7670.

Taghdirian, M. (2011). *Exponential Basis Functions (EBFs) in Solution of Fluid-Saturated Porous Media Differential Equations.* M. Sc. thesis, Isfahan University of Technology, Isfahan, Iran.

Vuyst, T. D., R. Vignjevic and J. C. Campbell (2005). Coupling between meshless and finite element methods. *International Journal of Impact Engineering* 31, 1054–1064.

Wang, Ch. and G. Wu (2011). A Brief Summary of Finite Element Method Applications to Nonlinear Wave-structure Interactions. *Journal of Marine Science and Application* 10, 127-138.

Wolfram Research, Inc., Mathematica, Version 9.0, Champaign, IL (2012).

Zandi, S. M., A. Rafizadeh and A. Shanehsazzadeh (2017). Numerical simulation of non-breaking solitary wave run-up using exponential basis functions. *Environmental Fluid Mechanics* 17, 1015-1034.

Zandi, S. M., B. Boroomand and S. Soghrati (2012b). Exponential basis functions in solution of problems with fully incompressible materials: A mesh-free method. *Journal of Computational Physics* 231, 7255–7273.

Zandi, S. M., B. Boroomand and S. Soghrati (2012a). Exponential basis functions in solution of incompressible fluid problems with moving free surfaces. *Journal of Computational Physics* 231, 505–527.

Zhang, A., P. Sun, F. Ming and A. Colagrossi (2017). Smoothed particle hydrodynamics and its applications in fluid-structure interactions. *Journal of Hydrodynamics* 29, 187-216.